Journal of
Materials Chemistry A

ROYAL SOCIETY OF CHEMISTRY

PAPER

View Article Online
View Journal | View Issue

Cite this: J. Mater. Chem. A, 2017, 5, 7118

Published on 14 March 2017. Downloaded by Peking University on 4/22/2023 8:17:02 AM.

Optimizing CdTe–metal interfaces for high performance solar cells†

Sibai Li, Zhi Peng, Jiaxin Zheng* and Feng Pan *

Received 21st January 2017
Accepted 13th March 2017

DOI: 10.1039/c7ta00698e

rsc.li/materials-a

CdTe is widely applied in thin film solar cells as a p-type layer, which is usually in contact with a metal back electrode. Using *ab initio* energy band calculations, here we study the interfacial properties of CdTe (110)–metal interfaces (metals = Al, Ag, Au, Cu, and Ni) systematically. Weak chemisorption and large interfacial distances are found between CdTe and Al, Ag and Cu surfaces, while medium or strong chemisorption and small interfacial distances are found between CdTe and Au and Ni surfaces. After GW correction, it is found that CdTe forms n-type Schottky contacts with Ag, Al and Cu and p-type Schottky contacts with Au and Ni at the interface between metalized CdTe and semiconductive CdTe, consistent with previous experimental values. Besides the Schottky barrier, tunneling barriers also exist at the CdTe–metal contact interface. The potential profiles at the vertical CdTe–metal interfaces reveal that due to the medium or strong chemisorption, tunneling barrier is absent at CdTe–Au and CdTe–Ni contacts, while the weak bonding interfaces (Ag, Al and Cu) have obvious tunneling barriers. Finally, methods to optimize the interface of the CdTe–metal contact to further decrease the Schottky barrier at the CdTe–metal contact are discussed.

Introduction

Due to its ideal band gap (1.51 eV)[1] for solar terrestrial photoconversion, CdTe is a well-known p-type layer material in thin film solar cells, which possesses a representative device structure: front electrode/n-type layer/p-type layer/back electrode. Besides the CdTe p-type layer in such a CdTe solar cell device, transparent conducting films (TCFs) such as FTO, ITO and AZO are usually used as the front electrode, CdS is often used as the n-type layer,[2–5] and different kinds of metal thin films such as Cu, Al, Ag, Au, and Ni are used as the back electrode.[6–13] A finite Schottky barrier usually appears at the interface between the CdTe layer and metal layer, which would lower the carrier transfer efficiency and decrease the power conversion efficiency (PCE). Therefore, it is important to decrease the Schottky barrier height (SBH) by optimizing the contact interfaces between thin films to enhance the performance of a solar cell. Unfortunately, the SBH does not simply depend on the work function of metals and the band structure of the semiconductor layer because of the complex interfacial properties. Many other factors, including interface reconstruction, surface states, and Fermi level pinning may influence the SBH. Thus understanding the interfacial properties between CdTe and the metal layer is crucial, which would provide helpful clues on how to optimize the contact interface between thin films.

The properties of CdTe–metal interfaces have been partly studied experimentally,[14–20] and theoretical research is limited. Recently, using first-principles calculations, Odkhuu *et al.* studied the formation energies and SBHs of interfaces between Cd(Zn)Te (111) and different layers of Cu, Pt and Al.[21] However, CdTe in the (110) orientation also has a high stability and is commonly used in experiments,[18,20,22,23] and some other metals (*e.g.*, Au and Ni) are also adopted as the back electrode in CdTe solar cells.[12,13] Apparently, interfaces between more metals and different crystal faces are worth studying.

Herein, using first-principles electronic band simulations, we explore the interfacial properties of CdTe (110) on high function metals (Au and Ni) and low function metals (Al, Ag and Cu) systematically for the first time. It is found that the binding energy of CdTe–Ni is obviously larger than those of other materials, which leads to a strong distortion of the interface and the disappearance of the tunneling barrier. In consideration of the GW correction and metallization of CdTe, an n-type Schottky contact is formed between CdTe and Al, Cu and Ag with an SBH of 0.12, 0.63 and 0.26 eV, respectively, and a p-type Schottky contact comes into being between CdTe and Au and Ni with an SBH of 0.44 and 0.66 eV, respectively. It is also found that the weak bonding interfaces (Ag, Al and Cu) have obvious tunneling barriers, which is another important character of a semiconductor–metal contact, while the medium or strong bonding interface (Au and Ni) has no tunneling barrier due to the strong orbital hybridization between Au/Ni and CdTe.

School of Advanced Materials, Peking University, Shenzhen Graduate School, Shenzhen 518055, China. E-mail: zhengjx@pkusz.edu.cn; panfeng@pkusz.edu.cn

† Electronic supplementary information (ESI) available. See DOI: 10.1039/c7ta00698e

 This journal is © The Royal Society of Chemistry 2017

Published on 14 March 2017. Downloaded by Peking University on 4/22/2023 8:17:02 AM.

Methodology

We use six layers of metal atoms to simulate the metal surface and build a supercell with six-layer CdTe adsorbed on the metal surface. The use of six-layer atoms to model the metal surfaces can give converged properties of the contact system for the convergence tests done in the previous studies.[24–26] The lattice parameters of (110)-CdTe are $a = 6.48$ Å and $b = 9.16$ Å. Apparently, the upper and the lower (110) surface of CdTe are symmetric, so the (110) surface is nonpolar. We use Virtual NanoLab version 2016.1, QuantumWise A/S to model the contact systems. Metals in the (110) orientation rather than in the (111) orientation are chosen in order to match (110)-CdTe well, because the former have square lattices the same as (110)-CdTe while the latter have hexagonal lattices. The (110)-CdTe 2 × 1 unit cell is adjusted to the $2\sqrt{2} \times 2\sqrt{2}$ unit cells of metals. The lattice mismatch of each metal is listed in Table 1, and ranges from 4.1–5.6%. To prevent spurious interaction between periodic images, a vacuum buffer space is set with the value of at least 15 Å. The topmost two-layer atoms of metal mainly interact with the topmost two-layer CdTe atoms, so the bottom four layers of metal and CdTe atoms are fixed in x and y directions.

We use a plane wave basis set and projector augmented wave (PAW)[27,28] method implemented in the Vienna ab initio simulation package (VASP)[29,30] code to optimize the structures. The generalized gradient approximation (GGA) functional to the exchange–correction functional of the Perdew–Burke–Ernzerhof (PBE)[31] form is adopted. The plane-wave cut off energy is set to 450 eV to ensure accuracy. The Brillouin zone is sampled by using 3 × 3 × 1 special k-points for optimizing these structures and 7 × 7 × 1 to get the densities of states (DOSs) and potential using the Monkhorst Pack scheme.[32] van der Waals interactions are taken into account, with the vdW-DF level of the optB88 exchange functional (optB88-vdW).[33] To obtain reliable optimized structures, the maximum residual force is less than 0.01 eV Å^{-1} and energies are converged to within 1×10^{-5} eV per atom. Using DFT+U with $U = 13$ eV (ref. 34) can reproduce the experimental lattice parameters of bulk CdTe. The reconstruction of (110)-CdTe is observed in previous research studies[35,36] and our calculation. We test different values of U to optimize the surface of (110)-CdTe and compare the predicted surface atomic geometry with the results of low-energy electron diffraction (LEED) intensity analysis.[36] As Fig. S3† shows, the PBE functional provides the best surface parameters except that $z1$ changes a little with increasing U value. So we did not choose the DFT+U method to further calculate the electronic structures of CdTe–metal systems. And the first-principles many-electron Green function approach within the GW approximation[37] is employed to calculate the band gap of CdTe to improve the electronic structure calculation performed using DFT.

Results and discussion

Geometry and stability of CdTe–metal interfaces

In general, a high-symmetry configuration is more stable than a low-symmetry one and often selected as the initial configuration. We have considered all the possible stacking configurations with high symmetry. After structure optimization, the energy of the configuration shown in Fig. S1† is lowest, so we choose it for subsequent calculations. Table 1 is the summary of the calculated key results of CdTe–metal interfaces studied in this work. The optimized interfacial structures are shown in Fig. 2. The equilibrium interfacial distance $d_{\mathrm{CdTe-M}}$ is defined as the difference between the average z-coordinates (vertical to the interface) of the bottom layer Cd and Te atoms and the top-most layer metal atoms (Fig. 1a). This varies from 1.14–2.30 Å decreasing in the order of Al > Cu > Ag > Au > Ni. The binding energy per interfacial Cd or Te atom is defined as

$$E_{\mathrm{b}} = (E_{\mathrm{CdTe}} + E_{\mathrm{metal}} - E_{\mathrm{CdTe-metal}})/N_{\mathrm{Cd}} \quad (1)$$

where E_{CdTe}, E_{metal}, and $E_{\mathrm{CdTe-metal}}$ are the relaxed energies of the CdTe surface, the metal surface, and the CdTe–metal system, respectively, and N_{Cd} is the number of interfacial Cd atoms in a supercell. The E_{b}, varying from 1.25–2.80 eV, increases in the order of Ag < Al < Cu < Au < Ni. The higher E_{b} corresponds to shorter $d_{\mathrm{CdTe-M}}$. Considering $d_{\mathrm{CdTe-M}}$ and E_{b}, the adsorption of CdTe–metal interfaces is classified into two types. Al, Ag and Cu have weak adsorption and large interfacial distances with CdTe ($E_{\mathrm{b}} = 1.25$–1.35 eV and $d_{\mathrm{CdTe-M}} = 2.27$–$2.30$ Å). Au has a medium adsorption and interfacial distance with CdTe ($E_{\mathrm{b}} = 1.58$ eV and $d_{\mathrm{Se-M}} = 1.96$ Å). Ni has a strong adsorption and short interfacial distance with CdTe ($E_{\mathrm{b}} = 2.80$ eV and $d_{\mathrm{Se-M}} = 1.14$ Å). In comparison with those of other

Table 1 Calculated interfacial properties of CdTe on metal surfaces. The lattice mismatch is ε. The equilibrium distance $d_{\mathrm{CdTe-M}}$ is the average distance between the surface Cd and Te atoms and relaxed positions of the topmost metal layer in the direction vertical to the interfaces. E_{b} is the binding energy. W_{M} and W are the calculated work functions of the clean metal surface and the metal surface adsorbed by CdTe, respectively. Φ_{C} is the SBH obtained from *ab initio* band calculations. Φ_{Exp} is the SBH obtained from experiments. The work function of CdTe is 5.21 eV. ΔV, w_{B}, and T_{B} are the tunneling barrier height, tunneling barrier width, and tunneling possibility, respectively

Metal	ε (%)	$d_{\mathrm{CdTe-M}}$ (Å)	E_{b} (eV)	W_{M} (eV)	W (eV)	Φ_{C} (eV)	Φ_{Exp} (eV)	w_{B} (Å)	ΔV (eV)	T_{B} (%)	Ref.
Al	5.0	2.30	1.35	4.22	4.05	0.12^{a}	0–0.40^{a}	0.49	1.41	56.7	22
Ag	5.6	2.27	1.25	4.21	4.19	0.26^{a}	0.69–1.00^{b}	0.51	1.87	49.0	20
Au	5.5	1.96	1.58	5.02	4.97	0.44^{b}	0.59–0.90^{b}	0	0	100	20 and 22
Cu	4.2	2.29	1.26	4.31	4.56	0.63^{b}	0.90–1.30^{b}	0.44	1.68	55.8	20
Ni	4.1	1.14	2.80	4.77	4.74	0.66^{b}	0.40–0.70^{a}	0	0	100	22, 23 and 46

^{a} For electron SBH. ^{b} For hole SBH.

Published on 14 March 2017. Downloaded by Peking University on 4/22/2023 8:17:02 AM.

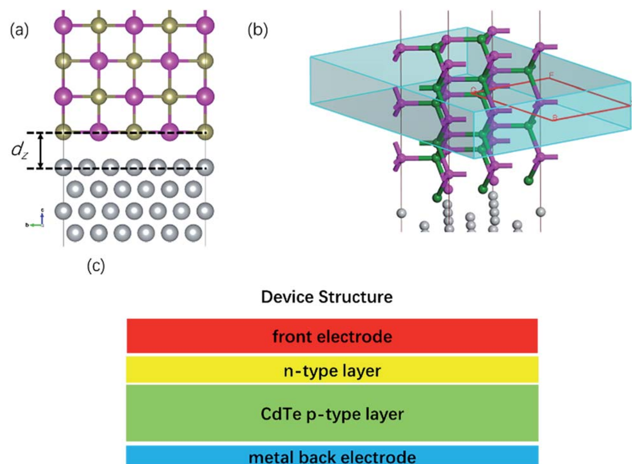

Fig. 1 Interfacial structures of CdTe–metal systems. The purple, green and light gray balls represent Cd, Te and metal atoms, respectively. (a) Side views of the first configuration of CdTe on the metal surfaces. (b) The Brillouin zone of CdTe–metal systems. Top view of the first configuration of CdTe on the metal surfaces. (c) Schematic diagram of a CdTe solar cell. Top view of the second configuration of CdTe on the metal surfaces. The purple, green and light gray balls represent Cd, Te and metal atoms, respectively.

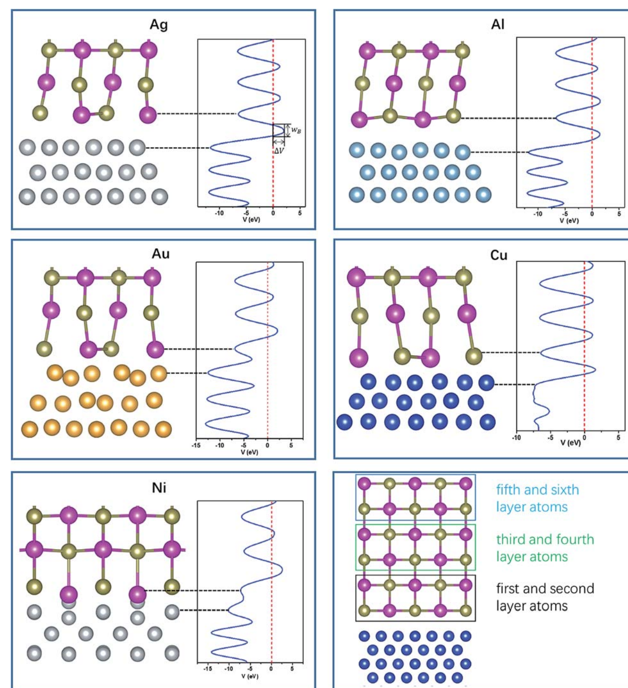

Fig. 2 Side view (from a-axis) of the optimized structures and average effective potentials in planes normal to the interface of CdTe–Ag, Al, Au, Cu and Ni systems, respectively. ΔV is the height of the barrier and w_B is the full width at half-maximum (fwhm) of the potential barrier. The Fermi level is set to zero. The last figure shows different layers of CdTe atoms on metal surfaces.

semiconductor–metal interfacial systems, such as phosphorene–metal[38] and $MoSe_2$–metal,[25] the binding energy of CdTe–metal is obviously larger, which means that strong hybridization occurs in these systems.

Electronic structures of CdTe–metal interfaces

The band structures of the interfacial systems and free-standing CdTe are shown in Fig. 3. The direct band gap at the Γ point of the free-standing CdTe is 0.87 eV, which is much smaller than the experimental value of 1.51 eV (ref. 1) and a little larger than the previous DFT value of 0.63 eV.[34,39] A feasible method to determine the accurate band edge position of the semiconductor is the first-principles many-electron Green function approach within the GW approximation, which can also produce a band gap consistent with experimental values. We suppose that the change of energy between E_f and the energy between the valence band maximum (VBM) or the conduction band minimum (CBM) is in proportion to the change of band gap after GW correction, E_C^{GW} and E_V^{GW} can be obtained as follows:

$$E_C^{GW} = E_f + \frac{E_C^{DFT} - E_f}{E_g^{DFT}} \times E_g^{GW}$$

$$E_V^{GW} = E_f + \frac{E_f - E_V^{DFT}}{E_g^{DFT}} \times E_g^{GW}$$

where E_g^{GW} is the band gap of CdTe obtained by GW approximation, and E_f, E_C^{DFT}, E_V^{DFT} and E_g^{DFT} are the Fermi level, CBM, VBM and band gap of CdTe obtained through the DFT calculation, respectively. Based on the unchanged Fermi level, this correction method has been used to obtain the absolute band position in previous studies.[26,40,41] The band gap of pure CdTe calculated by the GW method is 1.47 eV, which is consistent with the experiments. The Fermi level difference of CdTe calculated by DFT and GW methods is only 0.02 eV, so this correction method is applicable for CdTe.

As shown in Fig. 3, the band structures of CdTe are destroyed on all the metal surfaces, indicating an orbital hybridization and chemical bonding between CdTe and these metals. Because the Fermi level always crosses the CdTe derived band, part of CdTe (in contact with the metal) undergoes metallization. In contrast, the band structures of graphene on metals are not destroyed, some band structures of $MoSe_2$ on metals are destroyed and all band structures of phosphorene on metals are destroyed.[25,38] This difference indicates that the interactions between CdTe and the metal surface are stronger than those of graphene and $MoSe_2$ with metal surfaces.

To deeply understand the hybridization degree of the band structures of CdTe adsorbed on metals, we further calculate the partial density of states (PDOS) on Cd and Te orbitals of CdTe–metal systems, as shown in Fig. 4. Large amounts of CdTe states distribute in the original band gap of CdTe in all the interfacial systems, indicating the metallization of CdTe at these surfaces. It is mainly the Te p and Cd s states that arise in the pristine band gap of CdTe, while the Te s, Cd p and Cd d states only change a little. The PDOS at the E_f of the CdTe–Ni system is the largest among all the contact systems, which is consistent with the band structure hybridization degree. The different hybridization degrees can be illustrated by the different occupied

This journal is © The Royal Society of Chemistry 2017

Published on 14 March 2017. Downloaded by Peking University on 4/22/2023 8:17:02 AM.

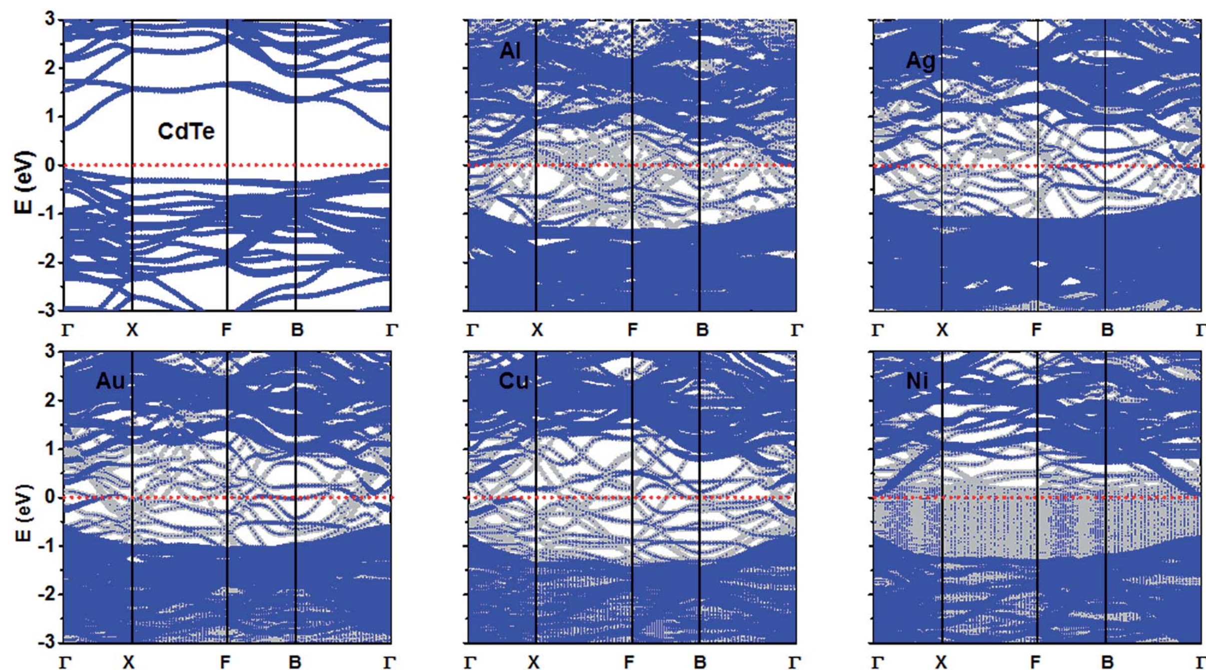

Fig. 3 Band structures of pure CdTe and CdTe–Al, Ag, Au, Cu and Ni contacts, respectively. Grey line: band structures of CdTe–metal systems; blue line: band structures of CdTe. The line width is proportional to the weight. The Fermi level is at zero energy.

levels of d-orbitals of metals. Al has unfilled d-orbitals and Cu, Ag and Au have fully filled d-orbital, so it's hard for them to form strong covalent bonds with the orbitals of the contacted Te atoms. Cu has a smaller d-orbital radius than Ag, so it has a stronger hybridization degree, while Ni has partially filled d-orbitals, which makes the binding energy of CdTe and Ni larger than those of other systems. Fig. 5 shows the PDOS of different layer atoms of CdTe of CdTe–metal systems. The first and second layer atoms of CdTe undergo obvious metallization, while the fifth and sixth layer atoms of CdTe almost retain their semiconductor nature.

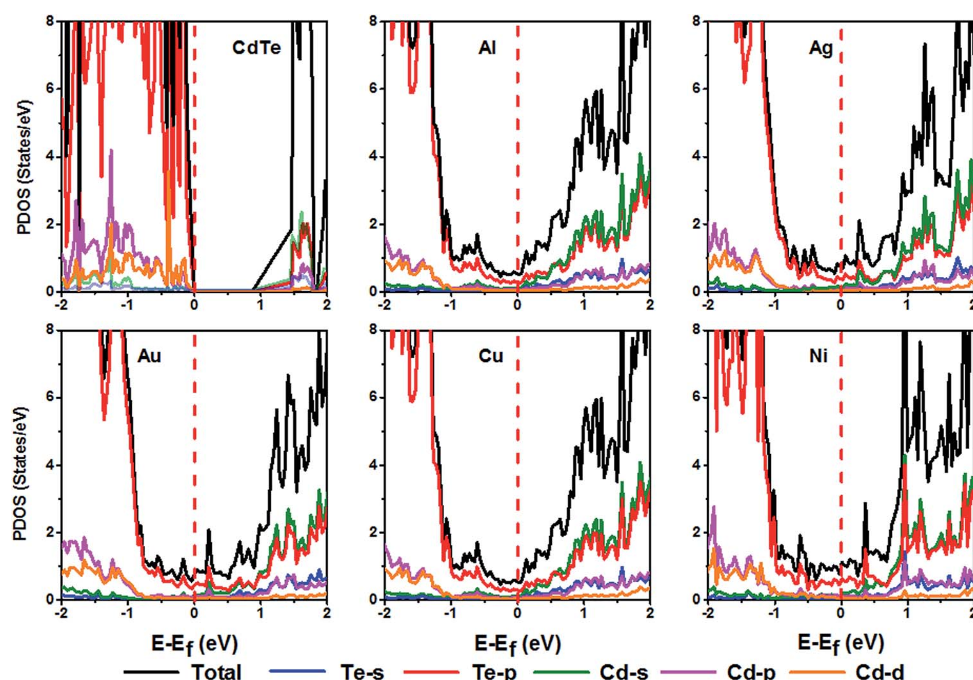

Fig. 4 Partial density of states (PDOS) (DOS on specified atoms and orbitals, for example, Cd-s (s-orbital on Cd)) of CdTe on the Al, Ag, Au, Cu and Ni surfaces at the DFT level. The Fermi level is at zero energy (red dashed line). The PDOS of free-standing CdTe is provided for comparison.

Published on 14 March 2017. Downloaded by Peking University on 4/22/2023 8:17:02 AM.

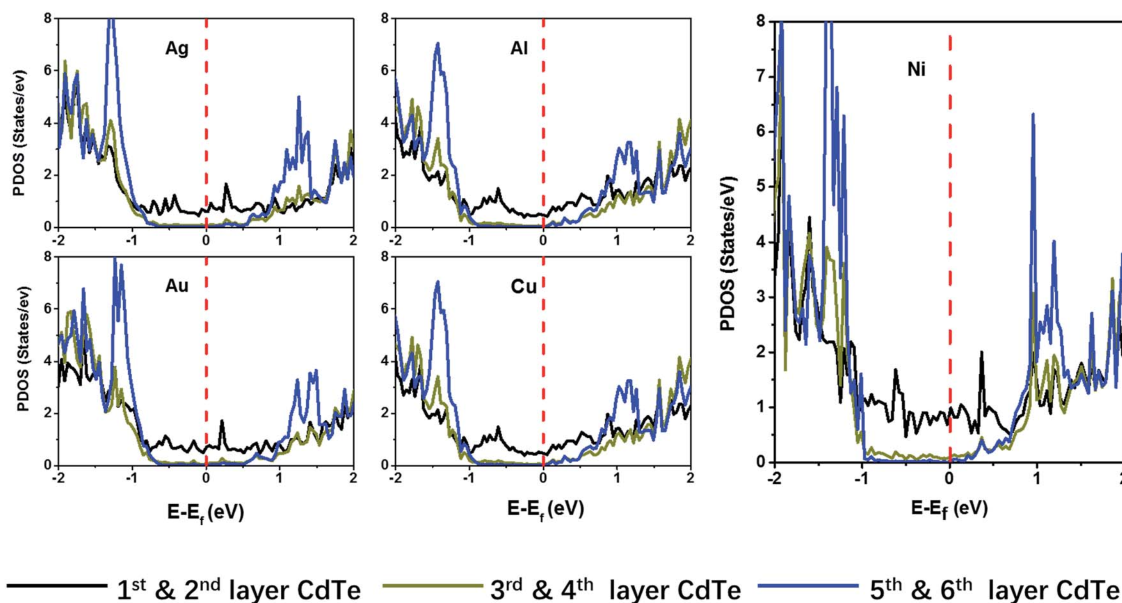

Fig. 5 PDOS of different layer atoms of CdTe on the Al, Ag, Au, Cu and Ni surfaces (see Fig. 2) at the DFT level. The Fermi level is at zero energy (red dashed line).

Schottky barrier and tunneling barrier of the contact between CdTe and metals

The schematic diagram of CdTe and a metal solar cell is shown in Fig. 6a. Schottky barriers may exist at either of two different interfaces of a CdTe solar cell: one is between the metal and CdTe contacted surface (labeled interface B), and the other is between metalized CdTe and semiconductive CdTe (labeled interface D). According to the band structure and PDOS analysis above, the strong interaction between CdTe and the metal makes CdTe contacted with metal come into metalization. So the Schottky barrier is absent at interface B and only appears at interface D. Because the fifth and sixth layer atoms of CdTe almost retain their semiconductor nature, we suppose that the interface D is between the fourth and the fifth layer of CdTe. It should be noted that though there is no Schottky barrier at interface B, the tunneling barrier would exist at interface B when electrons or holes cross the gap between the metal and CdTe. Fig. 6b shows the schematic diagram of band bending and illustrates the appearance of the tunneling barrier and Schottky barrier.

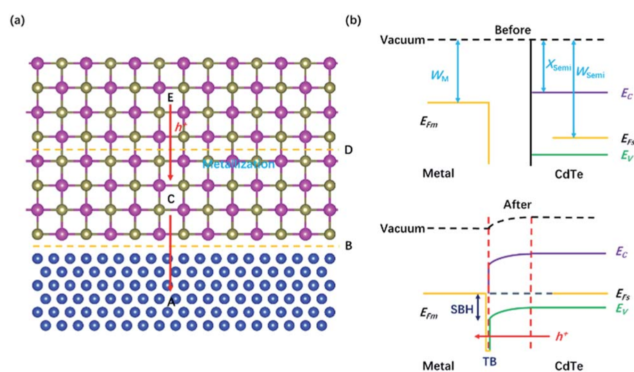

Fig. 6 (a) Schematic cross-sectional view of a typical metal contact to CdTe. A, C, and E denote three regions, while B and D are the two interfaces separating them. The red rows show the pathway (E → D → C → B → A) of hole injection from CdTe (E) to the metal (A). (b) Illustrations of the band bending of p-type SBHs that occurs at CdTe and metal contacts. E_{Fm} and E_{Fs} denote the Fermi level of the interfacial systems or metal and CdTe, respectively.

Fig. 7a shows the line-up of the metal Fermi level with the electronic bands of CdTe before and after GW correction. The calculated work function and the electron affinity of CdTe after GW correction are 5.21 and 3.93 eV, respectively, close to the experimental work function of 5–5.7 eV and the electron affinity of 4.28 eV.[22] As shown in Fig. 7b, the SBHs obtained by *ab initio* energy band calculation and experiment are very close. In particular, CdTe and Al form a quasi-ohmic contact with SBH $\Phi = 0.12$ eV for electrons in our calculation, consistent with some previous experiments where ohmic contact for electrons is formed between CdTe and Al.[18,42] Since CdTe is a p-type layer in solar cell, SBHs for hole between CdTe and metal is the property which we care for. The SBHs for holes decrease in the order of Al (1.35 eV) > Ag (1.21 eV) > Cu (0.84 eV) > Ni (0.66 eV) > Au (0.44 eV). Due to its smallest Schottky barrier for holes, using Au as the back electrode may produce the best performance among these metal candidates for the back electrode.

The tunneling barrier is another important character of a semiconductor–metal contact. The potential profiles at the vertical CdTe–metal interfaces are shown in Fig. 2. The weak bonding interfaces (Ag, Al and Cu) have obvious tunneling barriers, while the strong bonding interfaces (Au and Ni) have no tunneling barrier due to the strong orbital hybridization between Au/Ni and CdTe. The barrier height of CdTe–Ag, Al and Cu is 1.87, 1.41 and 1.68 eV, respectively. We use a square potential barrier to estimate the real potential barrier. The tunneling probability T_B is defined by[43]

This journal is © The Royal Society of Chemistry 2017

Published on 14 March 2017. Downloaded by Peking University on 4/22/2023 8:17:02 AM.

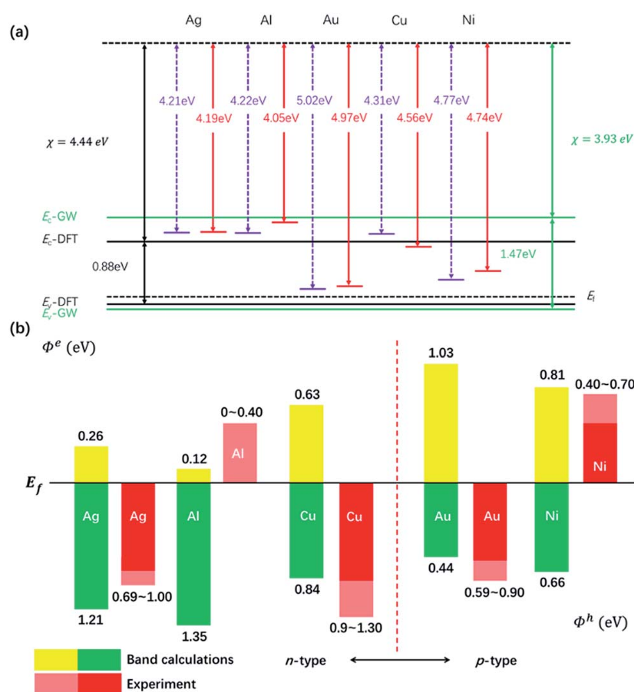

Fig. 7 (a) Line-up of the work functions with DFT and GW-corrected electronic bands of CdTe. The blue dashed line is the work function of the pure metal, and the red solid line is the work function of contacted systems (metal and 1–4 layer CdTe). (b) Comparison of the Schottky barrier heights (ϕ^e for electrons and ϕ^h for holes) of CdTe–Ag, Al, Cu, Au and Ni systems, respectively, obtained from both *ab initio* electronic band calculations and experiments.

$$T_B = \exp\left(-2\frac{\sqrt{2m\Delta V}}{\hbar} \times w_B\right)$$

where m is the mass of the free electron, $\hbar$ is the reduced Planck's constant, ΔV is the height of the barrier and w_B is the full width at half-maximum (fwhm) of the potential barrier as shown in Fig. 2. The resulting T_B values are 49.0, 55.8, 56.7, 100 and 100% for CdTe–Ag, Cu, Al, Au and Ni contacts, respectively. Thus the strong bonding between CdTe and Ni causes electrons or holes to transfer freely.

Discussion

From the above calculations, we can see that Schottky barriers exist in all the interfaces of CdTe–metal contacts. Even for Au, which possesses the smallest SBH for holes, the barrier is as high as 0.44 eV. To further improve the PCE of CdTe solar cells, methods are developed to optimize the interface of the CdTe–metal contact. For example, when Cu is used as the back electrode, controllable Cu diffusion into the CdTe surface layer is usually adopted by annealing to form Cu_2Te between CdTe and the Cu back electrode in devices.[44] For this reason, we also calculate the properties of the CdTe–Cu_2Te interface, as shown in Fig. 8. The binding energy E_b is 2.13 eV and the equilibrium interfacial distance d_{CdTe-M} is 2.25 Å. The covalent bonds formed between Cd and Te at the interface, which have a similar bond length (2.99 Å at the interface *vs.* 2.87 Å in CdTe) to the

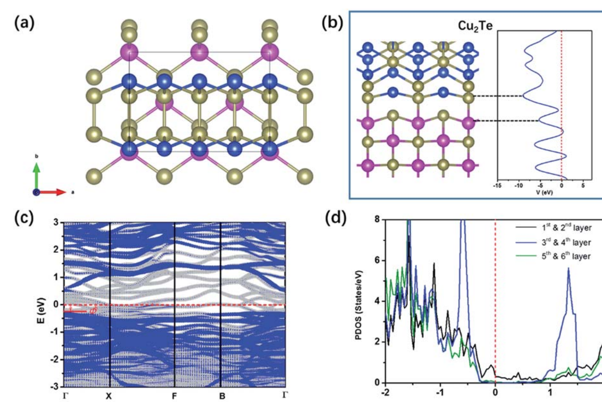

Fig. 8 (a) Top view of the configuration of CdTe on the Cu_2Te surfaces. (b) Side view (from *a*-axis) of the optimized structures and average effective potentials in planes normal to the interface of CdTe–Cu_2Te systems. (c) Band structures of CdTe–Cu_2Te systems; blue line: band structures of CdTe. The line width is proportional to the weight. The red arrow shows the SBH. (d) PDOS of different layer atoms of CdTe on the Cu_2Te surface at the DFT level. The Fermi level is set to zero.

Cd–Te bonds in bulk CdTe, lead to the high binding energy and the medium equilibrium interfacial distance. Apparently, the tunneling barrier is absent at the CdTe–Cu_2Te contact, which ensure the high efficiency of hole injection. The SBH for holes can be extracted from the band structure by comparing the Fermi level and the identifiable band edge of CdTe at the CdTe–Cu_2Te contact. From Fig. 8c, Φ^h and Φ^e are 0.37 eV and 0.50 eV, respectively. Using GW correction, Φ^h and Φ^e can be corrected to 0.63 eV and 0.84 eV, respectively. Compared with the CdTe–Cu contact, the hole SBH of the CdTe–Cu_2Te contact is Φ^h = 0.63 eV, while Φ^h = 0.84 eV at the CdTe–Cu contact, and the tunneling probability T_B of the CdTe–Cu_2Te contact is 100% while T_B = 55.8% at the CdTe–Cu contact. So the diffusion of Cu and formation of Cu_2Te would obviously improve the performance of the device. Recently, we used Cu_9S_5 as a buffer layer between CdTe and Au films, which shows a very high PCE (11.3%).[45] This is because Cu_9S_5 can form ohmic contact with Au and produce a successive gradient-doping region by controllable Cu diffusion, which greatly reduces the contact Schottky barrier.

Conclusions

In summary, this work presented a systematic theoretical study of the physical properties of CdTe–Al, Ag, Au, Cu and Ni interfaces. The adsorption level can be classified into three categories: weak chemisorption at CdTe and Al, Ag and Cu contacts, medium chemisorption at the CdTe and Au contact, and strong chemisorption at the CdTe and Ni contact. The band structure of CdTe is destroyed in all cases due to the strong hybridization. All metals form Schottky contacts with CdTe, and the p-type SBHs decrease in the order of Al (1.35 eV) > Ag (1.21 eV) > Cu (0.84 eV) > Ni (0.66 eV) > Au (0.44 eV). In contrast, the weak bonding interfaces (Ag, Al and Cu) have an obvious tunneling

Published on 14 March 2017. Downloaded by Peking University on 4/22/2023 8:17:02 AM.

barrier, while the medium or strong bonding interfaces (Au and Ni) have no tunneling barrier due to the strong orbital hybridization between Ni and CdTe, leading to the tunneling probability T_B decreasing in the order Ni (100%) = Au (100%) > Al (56.7%) > Cu (55.8%) > Ag (49.0%). Finally, methods to optimize the interface of the CdTe–metal contact to further decrease the Schottky barrier at the CdTe–metal contact are discussed.

Acknowledgements

This work was supported by the National Materials Genome Project (2016YFB0700600), Guangdong Innovation Team Project (No. 2013N080), and Shenzhen Science and Technology Research Grant (No. ZDSY20130331145131323, JCYJ20140903101633318, and JCYJ20140903101617271).

Notes and references

1 G. Fonthal, L. Tirado-Mejía, J. I. Marín-Hurtado, H. Ariza-Calderón and J. G. Mendoza-Alvarez, *J. Phys. Chem. Solids*, 2000, **61**, 579–583.
2 V. P. Singh, O. M. Erickson and J. H. Chao, *J. Appl. Phys.*, 1995, **78**, 4538–4542.
3 H. Bi, F. Huang, J. Liang, X. Xie and M. Jiang, *Adv. Mater.*, 2011, **23**, 3202–3206.
4 K. Zweibel, *Science*, 2010, **328**, 699–701.
5 J. D. Major, R. E. Treharne, L. J. Phillips and K. Durose, *Nature*, 2014, **511**, 334–337.
6 D. L. Bätzner, A. Romeo, H. Zogg, R. Wendt and A. N. Tiwari, *Thin Solid Films*, 2001, **387**, 151–154.
7 N. Romeo, A. Bosio, V. Canevari and A. Podestà, *Sol. Energy*, 2004, **77**, 795–801.
8 C. R. Corwine, A. O. Pudov, M. Gloeckler, S. H. Demtsu and J. R. Sites, *Sol. Energy Mater. Sol. Cells*, 2004, **82**, 481–489.
9 A. Gupta, V. Parikh and A. D. Compaan, *Sol. Energy Mater. Sol. Cells*, 2006, **90**, 2263–2271.
10 S. H. Demtsu, D. S. Albin, J. W. Pankow and A. Davies, *Sol. Energy Mater. Sol. Cells*, 2006, **90**, 2934–2943.
11 A. Niemegeers and M. Burgelman, *J. Appl. Phys.*, 1997, **81**, 2881–2886.
12 U. Kaufmann, J. Windscheif and G. Brunthaler, *J. Phys. C: Solid State Phys.*, 1984, **17**, 6169.
13 K. Ernst, R. Engelhardt, K. Ellmer, C. Kelch, H.-J. Muffler, M.-C. Lux-Steiner and R. Könenkamp, *Thin Solid Films*, 2001, **387**, 26–28.
14 V. A. Gnatyuk, T. Aoki, Y. Hatanaka and O. I. Vlasenko, *Appl. Surf. Sci.*, 2005, **244**, 528–532.
15 J. L. Shaw, R. E. Viturro, L. J. Brillson and D. LaGraffe, *Appl. Phys. Lett.*, 1988, **53**, 1723.
16 A. E. Fowell, R. H. Williams, B. E. Richardson and T. H. Shen, *Semicond. Sci. Technol.*, 1990, **5**, 348–350.
17 H. Toyama, M. Yamazato, A. Higa, T. Maehama, R. Ohno and M. Toguchi, *Jpn. J. Appl. Phys., Part 1*, 2005, **44**, 6742–6746.
18 A. K. Wahi, *J. Vac. Sci. Technol., A*, 1990, **8**, 1926.
19 G. H. Parker and C. A. Mead, *Phys. Rev.*, 1969, **184**, 780–787.
20 S. E. Laboratories and S. Uniuersity, *Phys. Rev. B: Condens. Matter Mater. Phys.*, 1988, **37**, 731–739.
21 D. Odkhuu, M. S. Miao, F. Aqariden, C. Grein and N. Kioussis, *J. Appl. Phys.*, 2016, **120**, 185703.
22 T. Takabe, J. Saraie and T. Tanaka, *Phys. Status Solidi A*, 1978, **47**, 123–130.
23 M. H. Patterson and R. H. Williams, *J. Cryst. Growth*, 1982, **59**, 281–288.
24 Y. Wang, R. X. Yang, R. Quhe, H. Zhong, L. Cong, M. Ye, Z. Ni, Z. Song, J. Yang, J. Shi, J. Li and J. Lu, *Nanoscale*, 2016, 1179–1191.
25 Y. Pan, S. Li, M. Ye, R. Quhe, Z. Song, Y. Wang, J. Zheng, F. Pan, W. Guo, J. Yang and J. Lu, *J. Phys. Chem. C*, 2016, **120**, 13063–13070.
26 Y. Y. Pan, Y. Y. Wang, L. Wang, H. X. Zhong, R. G. Quhe, Z. Y. Ni, M. Ye, W. N. Mei, J. J. Shi, W. L. Guo, J. B. Yang and J. Lu, *Nanoscale*, 2015, **7**, 2116–2127.
27 P. E. Blöchl, *Phys. Rev. B: Condens. Matter Mater. Phys.*, 1994, **50**, 17953–17979.
28 G. Kresse and D. Joubert, *Phys. Rev. B: Condens. Matter Mater. Phys.*, 1999, **59**, 11–19.
29 G. Kresse and J. Furthmüller, *Comput. Mater. Sci.*, 1996, **6**, 15–50.
30 G. Kresse and J. Furthmüller, *Phys. Rev. B: Condens. Matter Mater. Phys.*, 1996, **54**, 11169–11186.
31 J. P. Perdew, K. Burke and M. Ernzerhof, *Phys. Rev. Lett.*, 1996, 3865–3868.
32 H. J. Monkhorst and J. D. Pack, *Phys. Rev. B: Condens. Matter Mater. Phys.*, 1976, **13**, 5188–5192.
33 J. Klimeš, D. R. Bowler and A. Michaelides, *Phys. Rev. B*, 2010, **22**, 22201.
34 Y. Wu, G. Chen, Y. Zhu, W. J. Yin, Y. Yan, M. Al-Jassim and S. J. Pennycook, *Comput. Mater. Sci.*, 2015, **98**, 18–23.
35 Y. R. Wang, C. B. Duke, K. O. Magnusson and S. A. Flodström, *Surf. Sci.*, 1988, **205**, L760–L770.
36 R. J. Meyer, C. B. Duke, A. Paton, J. L. Yeh, J. C. Tsang, A. Kahn and P. Mark, *Phys. Rev. B: Condens. Matter Mater. Phys.*, 1980, **21**, 4740–4750.
37 L. Hedin, *Phys. Rev.*, 1965, **139**, A796–A823.
38 Y. Pan, Y. Wang, M. Ye, R. Quhe, H. Zhong, Z. Song, X. Peng, D. Yu, J. Yang, J. Shi and J. Lu, *Chem. Mater.*, 2016, **28**, 2100–2109.
39 E. Menéndez-Proupin, A. Amézaga and N. Cruz Hernández, *Phys. Rev. B: Condens. Matter Mater. Phys.*, 2014, **452**, 119–123.
40 C. Gong, H. Zhang, W. Wang, L. Colombo, R. M. Wallace and K. Cho, *Appl. Phys. Lett.*, 2013, **103**, 53513.
41 H. Jiang, *J. Phys. Chem. C*, 2012, **116**, 7664–7671.
42 R. H. Williams and M. H. Patterson, *Appl. Phys. Lett.*, 1982, **40**, 484–486.
43 X. Ji, J. Zhang, Y. Wang, H. Qian and Z. Yu, *Phys. Chem. Chem. Phys.*, 2013, **15**, 17883–17886.
44 K. D. Dobson, I. Visoly-Fisher, G. Hodes and D. Cahen, *Sol. Energy Mater. Sol. Cells*, 2000, **62**, 295–325.
45 M. J. Zhang, Q. Lin, X. Yang, Z. Mei, J. Liang, Y. Lin and F. Pan, *Nano Lett.*, 2016, **16**, 1218–1223.
46 L. A. Kosyachenko, V. M. Sklyarchuk, O. F. Sklyarchuk, O. L. Maslyanchuk, V. A. Gnatyuk and T. Aoki, *IEEE Trans. Nucl. Sci.*, 2009, **56**, 1827–1834.

This journal is © The Royal Society of Chemistry 2017